JCI insight

# Splicing modulation sensitizes chronic lymphocytic leukemia cells to venetoclax by remodeling mitochondrial apoptotic dependencies

Elisa ten Hacken, … , Matthew S. Davids, Catherine J. Wu

*JCI Insight.* 2018;3(19):e121438. https://doi.org/10.1172/jci.insight.121438.

**Research Article** **Hematology** **Therapeutics**

The identification of targetable vulnerabilities in the context of therapeutic resistance is a key challenge in cancer treatment. We detected pervasive aberrant splicing as a characteristic feature of chronic lymphocytic leukemia (CLL), irrespective of splicing factor mutation status, which was associated with sensitivity to the spliceosome modulator, E7107. Splicing modulation affected CLL survival pathways, including members of the B cell lymphoma-2 (BCL2) family of proteins, remodeling antiapoptotic dependencies of human and murine CLL cells. E7107 treatment decreased myeloid cell leukemia-1 (MCL1) dependence and increased BCL2 dependence, sensitizing primary human CLL cells and venetoclax-resistant CLL-like cells from an Eμ-TCL1–based adoptive transfer murine model to treatment with the BCL2 inhibitor venetoclax. Our data provide preclinical rationale to support the combination of venetoclax with splicing modulators to reprogram apoptotic dependencies in CLL for treating venetoclax-resistant CLL cases.



JCI insight

RESEARCH ARTICLE

# Splicing modulation sensitizes chronic lymphocytic leukemia cells to venetoclax by remodeling mitochondrial apoptotic dependencies

**Elisa ten Hacken,[1] Rebecca Valentin,[1] Fara Faye D. Regis,[1] Jing Sun,[1] Shanye Yin,[2] Lillian Werner,[3] Jing Deng,[1] Michaela Gruber,[1] Jessica Wong,[1] Mei Zheng,[4] Amy L. Gill,[1] Michael Seiler,[5] Peter Smith,[5] Michael Thomas,[5] Silvia Buonamici,[5] Emanuela M. Ghia,[6] Ekaterina Kim,[7] Laura Z. Rassenti,[6] Jan A. Burger,[7] Thomas J. Kipps,[6] Matthew L. Meyerson,[1,8,9] Pavan Bachireddy,[1,8,10] Lili Wang,[1,8] Robin Reed,[2] Donna Neuberg,[3] Ruben D. Carrasco,[4,11] Angela N. Brooks,[12] Anthony Letai,[1,8,10] Matthew S. Davids,[1,8,10] and Catherine J. Wu[1,8,9,10]**

[1]Department of Medical Oncology, Dana-Farber Cancer Institute, Boston, Massachusetts, USA. [2]Department of Cell Biology, Harvard Medical School, Boston, Massachusetts, USA. [3]Department of Biostatistics and Computational Biology, Dana-Farber Cancer Institute, Boston, Massachusetts, USA. [4]Department of Pathology, Brigham and Women's Hospital, Boston, Massachusetts, USA. [5]H3 Biomedicine Inc., Cambridge, Massachusetts, USA. [6]Moores Cancer Center, University of California, San Diego, La Jolla, California, USA. [7]University of Texas MD Anderson Cancer Center, Houston, Texas, USA. [8]Harvard Medical School, Boston, Massachusetts, USA. [9]Broad Institute, Cambridge, Massachusetts, USA. [10]Department of Medicine, Brigham and Women's Hospital, Boston, Massachusetts, USA. [11]Department of Oncologic Pathology, Dana-Farber Cancer Institute, Boston, Massachusetts, USA. [12]Department of Biomolecular Engineering, University of California, Santa Cruz, California, USA.

**The identification of targetable vulnerabilities in the context of therapeutic resistance is a key challenge in cancer treatment. We detected pervasive aberrant splicing as a characteristic feature of chronic lymphocytic leukemia (CLL), irrespective of splicing factor mutation status, which was associated with sensitivity to the spliceosome modulator, E7107. Splicing modulation affected CLL survival pathways, including members of the B cell lymphoma-2 (BCL2) family of proteins, remodeling antiapoptotic dependencies of human and murine CLL cells. E7107 treatment decreased myeloid cell leukemia-1 (MCL1) dependence and increased BCL2 dependence, sensitizing primary human CLL cells and venetoclax-resistant CLL-like cells from an Eμ-TCL1–based adoptive transfer murine model to treatment with the BCL2 inhibitor venetoclax. Our data provide preclinical rationale to support the combination of venetoclax with splicing modulators to reprogram apoptotic dependencies in CLL for treating venetoclax-resistant CLL cases.**

**Conflict of interest:** PS, MS, MT, and SB are employees of H3 Biomedicine Inc. JAB received research funding from TG Therapeutics, Pharmacyclics, Gilead, Portola, and BeiGene and is a consultant for Janssen. TJK received research funding from Oncternal, AbbVie, Roche-Genentech, and Pharmacyclics; received honoraria from Gilead, Pharmacyclics, Celgene, and AbbVie; and is a consultant for Gilead, Pharmacyclics, Celgene, AbbVie, and Roche-Genentech. RV received travel reimbursement from AbbVie and Roche-Genentech. MSD received research funding from Pharmacyclics, TG Therapeutics, Roche-Genentech, Bristol Myers Squibb, and Surface Oncology and is a consultant for AbbVie, Pharmacyclics, TG Therapeutics, Roche-Genentech, Janssen, Merck, AstraZeneca, Incyte, and MEI Pharma. AL is a cofounder and scientific advisory board member of Leap Oncology and Flash Therapeutics and a consultant for AbbVie and Novartis. His laboratory receives research funding from AbbVie, AstraZeneca, Syros, and Novartis. CJW is a cofounder and scientific advisory board member of Neon Therapeutics and receives research funding from Pharmacyclics.



**Submitted:** April 2, 2018
**Accepted:** August 29, 2018
**Published:** October 4, 2018

**Reference information:**
*JCI Insight*. 2018;3(19):e121438.
https://doi.org/10.1172/jci.insight.121438.

## Introduction

The therapeutic landscape of the mature B cell malignancy chronic lymphocytic leukemia (CLL) has changed greatly over the last decade due to the introduction of novel inhibitors targeting its critical survival pathways, such as venetoclax, which potently inhibits the BCL2 signaling pathway (1). Despite the efficacy of venetoclax and other novel targeted inhibitors that have been recently approved by the FDA (2), therapeutic resistance is emerging as one of the foremost challenges in the clinical management of CLL. The identification of novel combinatorial treatment strategies that could induce deeper and more durable remissions is thus a high priority in preclinical and clinical investigations of CLL.

Recent genomic investigations of CLL have revealed novel driver alterations and affected cellular pathways of this malignancy (3, 4). From these studies, mutation in the gene encoding the RNA splicing factor 3b subunit 1 (*SF3B1*) has been identified as among the most common alterations in CLL and has been found to be associated with aberrant alternative splicing (5–10). Earlier studies have demonstrated CLL-specific accumulation of aberrantly spliced isoforms of B cell receptor signaling components (5, 11) or BCL2 family members (5, 12, 13) and, more recently, overexpression of spliceosome components in

CLL when compared with healthy donor B cells (14), although the extent to which aberrant splicing characterizes CLL oncogenic pathways remains incompletely defined.

We asked whether splicing modulation could perturb CLL prosurvival pathways, providing opportunities for novel combinatorial treatment strategies in the setting of treatment resistance.

## Results

*Aberrant splicing is a common feature of CLL and sensitizes CLL to splicing modulation*. We asked whether aberrant splicing was a characteristic feature of CLL cells, irrespective of *SF3B1* mutation status, and surveyed the spectrum of alternatively spliced events in CLL samples as compared with normal B cells. To this end, we reexamined our previously reported RNA-sequencing (RNA-seq) data set (10), focusing on the comparison of 22 primary CLL samples (9 *SF3B1*$^{mut}$ and 13 *SF3B1*$^{wt}$, Supplemental Table 1; supplemental material available online with this article; https://doi.org/10.1172/jci.insight.121438DS1) and CD19$^{+}$ normal B cells collected from 7 healthy adult volunteers. We applied two complementary analyses to define (a) the most differentially spliced events and (b) the total number of splicing outliers in CLL cells as compared with normal B cell samples.

We first identified and classified splice variants using the JuncBASE algorithm (15) and further used this tool to calculate for each variant a percent spliced in (PSI) value, which is a measure of the abundance of the inclusion isoform for each splice isoform category relative to the total abundance of all isoforms. We defined the most variable splicing in normal B and CLL cells as the events with the highest median absolute deviation in PSI (Supplemental Figure 1A). To identify differences between CLL and normal B cells, we used the same cutoffs for significance as we previously reported (FDR < 0.10 and $|\Delta PSI| > 10\%$) (10) and found 192 differentially spliced events significantly enriched in CLL cells compared with normal B cells, with intron retention (IR) as the most represented category (Figure 1A). The distribution of splice events based on their ΔPSI between CLL and normal B samples highlighted a proportional shift in abundance toward lower PSI values in the former (Figure 1B). Consistently, PSI values of IR events were lower in CLL samples compared with normal B cells (Figure 1C, $P = 0.0037$), indicating a lower presence of inclusion isoforms in the CLL samples and suggesting increased splicing of introns as a CLL-specific mechanism of transcriptional regulation.

In our second analysis, we asked whether individual CLL samples had generally elevated levels of aberrant splice events, which were not shared among all CLL samples, and thus would not have been identified through our differential splicing analysis. We defined outlier splicing events across normal B and CLL samples as those having a PSI value in the tenth percentile of all PSI values and greater than 10% compared with the median PSI for each individual event (Figure 1D). Strikingly, the overall extent of dysregulated splicing (i.e., total splicing outlier count) was greater in the CLL samples, irrespective of *SF3B1* mutation status, than in normal B cells ($P$ [normal B vs. CLL] < 0.0001; $P$ [normal B vs. *SF3B1*$^{wt}$] = 0.0004; $P$ [normal B. vs. *SF3B1*$^{mut}$] = 0.03). While the total number of splicing outliers did not significantly differ between *SF3B1*$^{mut}$ and *SF3B1*$^{wt}$ samples (Figure 1D, $P$ [*SF3B1*$^{wt}$ vs. *SF3B1*$^{mut}$] = 0.45), alternative 3′ splice site usage was enriched in *SF3B1*$^{mut}$ compared with *SF3B1*$^{wt}$ samples, as expected based on prior analyses (5, 7–10) (Supplemental Figure 1B). To identify signaling pathways affected by altered splicing in CLL compared with B cells, we performed Panther analysis (16) of the 192 most differentially spliced events between CLL cells and normal B cells and of the splicing outliers present in at least 7 of 22 CLL samples but absent from any of the normal B cell samples. This analysis revealed altered splicing to potentially affect pathways relevant to normal B cell biology and CLL lymphomagenesis, including the B cell activation, Wnt, Notch, interleukin signaling, and p53 pathways, as well as those related to general processes relevant to cellular homeostasis, including the oxidative stress response, hypoxia response via HIF, fatty acid, nucleotide biosynthesis, and ubiquitin-proteasome pathways (Figure 1E and Supplemental Table 2).

Altogether, these data suggested that aberrant splicing is a characteristic feature of CLL and that splicing modulation could be broadly effective across CLL samples. Consistent with these findings, we observed greater in vitro loss of viability in 20 independent CLL samples (10 *SF3B1*$^{wt}$ and 10 *SF3B1*$^{mut}$, Supplemental Table 3) compared with B cells from 5 healthy volunteers, following 8 hours of exposure to the splicing modulator E7107 (17) at concentrations ranging from 10 nM to 1 μM (Figure 1F, $P \leq 0.01$ across all comparisons of normal vs. CLL samples). Loss of viability in CLL samples was dose dependent and irrespective of *SF3B1* mutation status, in line with a previous report on fewer cases (18).

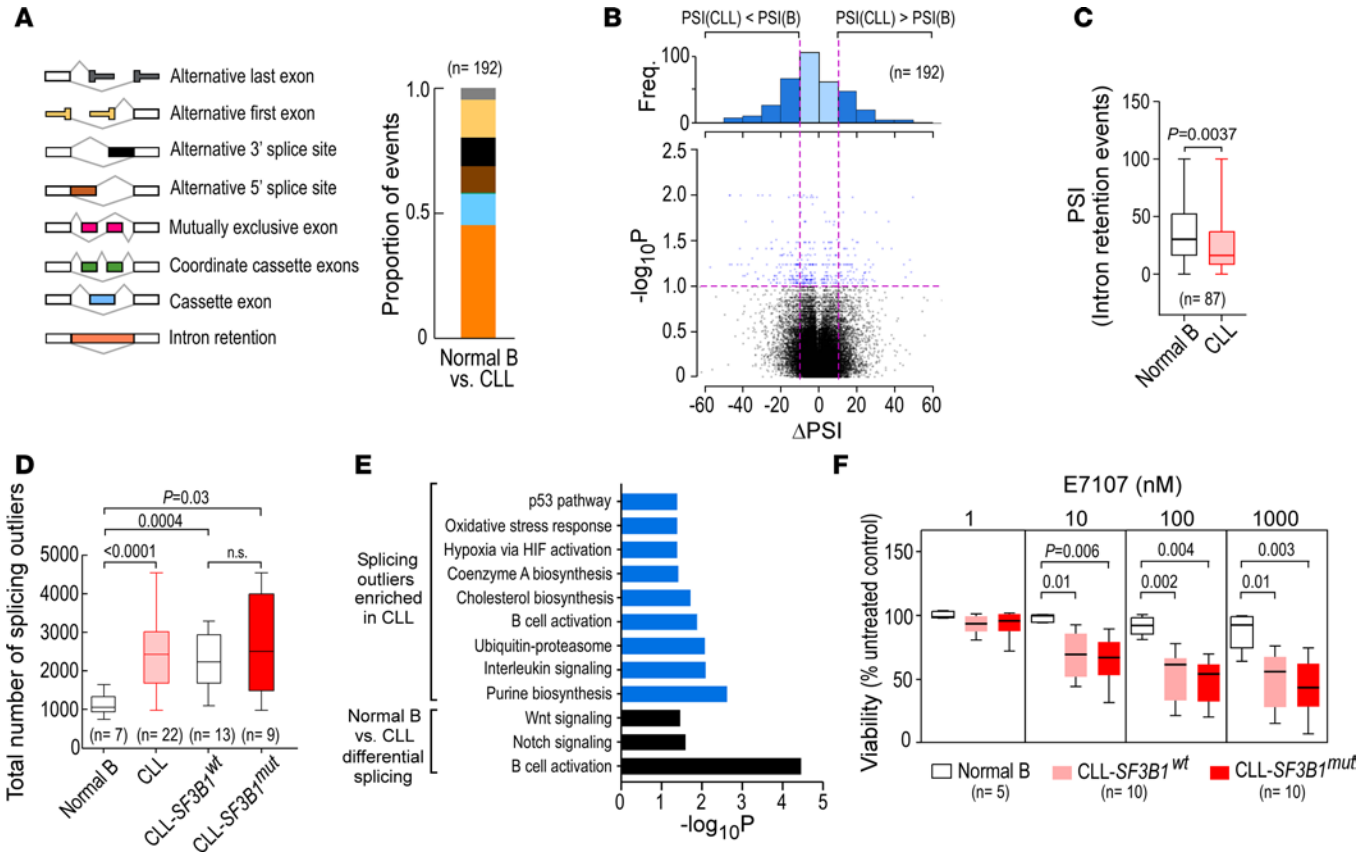


**Figure 1. Aberrant splicing is a general property of CLL, which underlies sensitivity to splicing modulation.** (**A**) Proportion of events within splicing categories of the 192 differential splice events based on analysis of RNA-seq data from 7 normal B cell samples and 22 CLL samples (13 CLL-*SF3B1*$^{wt}$ and 9 *SF3B1*$^{mut}$). (**B**) Distribution of splice events in 22 CLL samples compared with 7 CD19$^{+}$ cells based on Δ percent spliced in (ΔPSI) values versus negative logarithmic *P* values ($-\log_{10}P$) of all splicing changes. Pink and black dashed lines indicate thresholds of |ΔPSI| of 10% and FDR of 10% (i.e., $-\log_{10}P = 1$) for significant splice changes. Blue frequency bars indicate the number of significantly differential events in CLL as compared with normal B cells, of a total of 192. Light blue bars indicate nonsignificant events falling within the −10 < PSI < 10 interval. (**C**) PSI values of the 87 intron retention events within the 192 most differential splicing displayed in panel **A**. *P* value was calculated by Mann Whitney *U* test. (**D**) Total number of the top tenth percentile outlier splicing events across normal B cell and CLL samples, based on RNA-seq analysis. Reported *P* values were calculated by Welch *t* test with Bonferroni correction. (**E**) Pathway enrichment analysis by the Panther algorithm of the 192 most differential splicing events between CLL and normal B cells (black) and the CLL-specific splicing outliers represented in at least 7 of the 22 CLL samples (blue). Significantly enriched pathways within each category and respective $-\log_{10}P$ values are indicated in the figure. (**F**) Percentage viability of CD19$^{+}$ cells from 5 healthy donor PBMCs, 10 *SF3B1*$^{wt}$ CLL samples, and 10 *SF3B1*$^{mut}$ CLL samples after 8 hours of treatment with increasing concentrations of E7107 (1 nM to 1 μM). Reported *P* values were calculated by 1-way ANOVA with Scheffé's correction.

*The spliceosome modulator E7107 broadly affects the CLL transcriptome*. To comprehensively define candidate altered splice variants mediating this loss of viability in CLL cells following exposure to E7107, we performed transcriptome analysis of 11 primary CLL samples (6 *SF3B1*$^{wt}$ and 5 *SF3B1*$^{mut}$, Supplemental Table 3) exposed to 5 nM E7107 for 8 hours. This time frame allowed us to appreciate E7107-specific transcriptional changes, excluding confounding effects of cellular apoptosis. In line with the aforementioned observation of increased intronic splicing in CLL (Figure 1C), and with IR and cassette exon (CE) events being highly variable within CLL samples (Supplemental Figure 1A), we identified IR and CE as primary targets of E7107. We detected widespread increased IR and concomitant decreased CE inclusion across multiple targets (Figure 2A, FDR < 0.10 and |ΔPSI| > 10%, E7107 vs. DMSO), with no notable differences in the proportion of affected splice events based on *SF3B1* mutation status (Figure 2B and Supplemental Figure 2, A and B). To identify the key pathways affected by E7107 treatment, we again applied Panther analysis (16) to the 1,000 most significant IR and the 1,000 most significant CE events (ranking based on adjusted *P* value) and to the events with near maximal shifts in |ΔPSI| after E7107 treatment (i.e., |ΔPSI| > 90; *n* = 1,904). Six of eleven previously identified pathways enriched in CLL were also found to be enriched in E7107 targets, while seven additional ones with relevance to CLL biology were identified as targeted by E7107 (i.e., the Ras, apoptosis signaling,

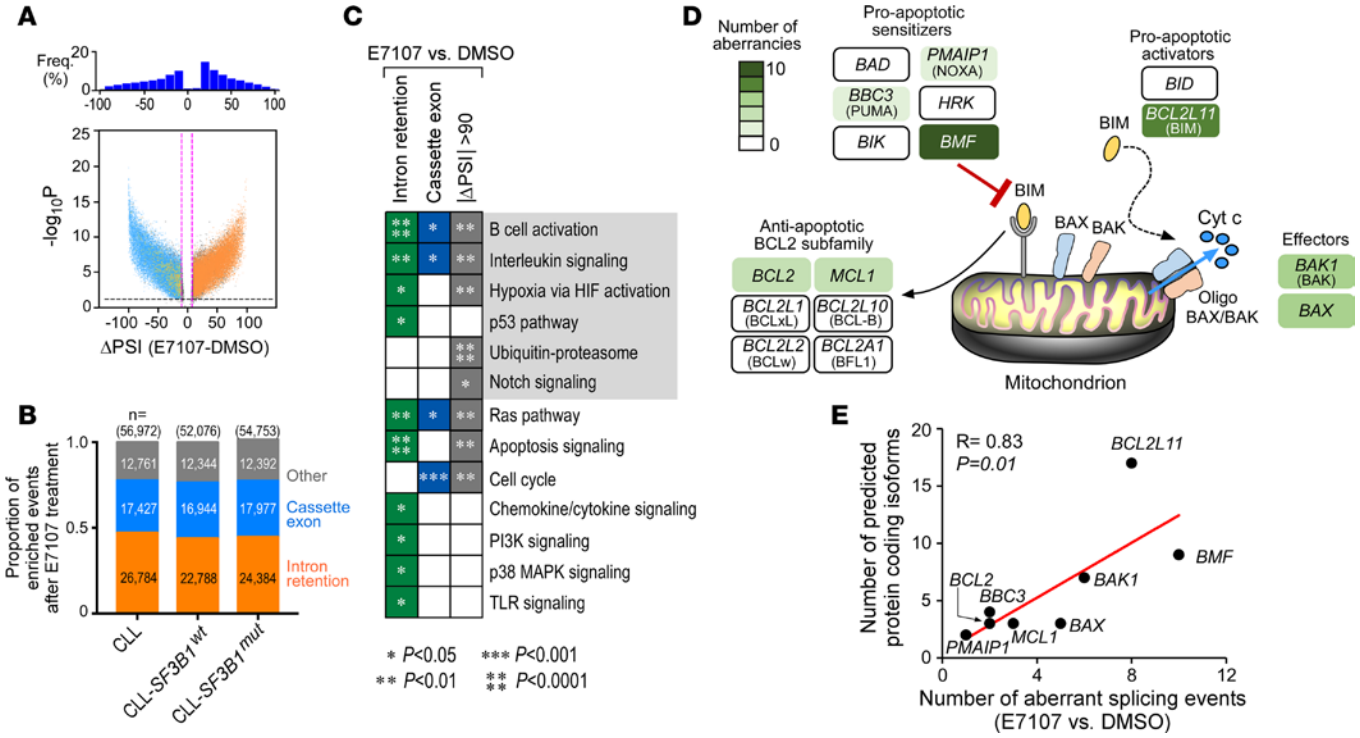


**Figure 2. Splicing modulation by E7107 treatment broadly affects the CLL transcriptome.** (**A**) Frequency of ΔPSI for significant splice changes from the RNA-Seq data of 11 CLL samples after 8 hours of treatment with 5 nM E7107 compared with DMSO-treated controls and volcano plot of ΔPSI versus negative logarithmic *P* values ($-\log_{10}P$) of all splicing changes. Pink and black dashed lines indicate thresholds of |ΔPSI| of 10% and FDR of 10% (i.e., $-\log_{10}P = 1$) for significant splice changes. Orange dots indicate significant intron retention events; light blue dots indicate significant cassette exon events; gray dots indicate all other categories of splice events. A similar analysis of CLL samples based on *SF3B1* mutation status is provided in Supplemental Figure 2, A and B. (**B**) Proportion of events within intron retention (orange), cassette exon (blue), and all other splicing categories (gray), and numbers of significantly (FDR < 0.10 and |ΔPSI| > 10%) modulated events by E7107 within all the 11 CLL samples or within samples divided based on *SF3B1* mutation status (6 $SF3B1^{wt}$, 5 $SF3B1^{mut}$). (**C**) Panther algorithm pathway enrichment analysis of the 1,000 most significant intron retention and the 1,000 most significant cassette exon events and the 1,904 events with |ΔPSI| > 90 after E7107 treatment as compared with DMSO control. Significant *P* values are indicated in the figure. The gray area shaded highlights pathways also enriched in Figure 1E. A similar analysis with a maximal stringency of |ΔPSI| = 100 for the third category is displayed in Supplemental Figure 2C. (**D**) Schematic representation of the BCL2 family members, colored based on the number of splicing aberrations induced by E7107 treatment (0, white; 10, dark green). Gene names are indicated in italics. When gene names differ from protein products, the respective protein name is indicated in parenthesis. (**E**) Linear regression of number of predicted protein-coding isoforms of BCL2 family members targeted by E7107 (*y* axis) and the number of splicing aberrancies induced by E7107 treatment (*x* axis). Spearman correlation *R* and *P* values are indicated in the figure.

cell cycle, chemokine/cytokine signaling, PI3K signaling, MAPK signaling, and TLR signaling pathways) (Figure 2C and Supplemental Table 4). Importantly, B cell activation and apoptosis signaling were significantly enriched, even at maximal stringency (i.e., |ΔPSI| = 100, 471 events, Supplemental Figure 2C). Of note, we identified *BTK* and *MCL1* among the intron-retained targets, *CD79B* and *CD19* among the CE-skipped events, and *PLCG2* and *BCL2L11* among the targets with a |ΔPSI| of 100.

*BCL2 family members are among the targets of E7107.* Since apoptotic signaling was one of the candidate pathways targeted by E7107, and because proapoptotic and antiapoptotic functions of BCL2 family members are tightly regulated by alternative splicing (19), we further analyzed the effect of E7107 on individual members of the BCL2 family of proteins. We enumerated the total number of splicing aberrancies of each of the proapoptotic and antiapoptotic members of the BCL2 family, using a more stringent cutoff of |ΔPSI| > 20%, and identified a total of 37 splicing aberrations, mostly IR increase and CE skipping, but also alternative 5′ or 3′ splice site usage, in *MCL1*, *BCL2*, *BAK1*, *BAX*, *PMAIP1* (the gene encoding for NOXA), *BBC3* (PUMA), *BMF*, and *BCL2L11* (BIM) (Figure 2D). The number of aberrantly spliced events was highly correlated with the total number of predicted protein-coding isoforms among annotated splice variants of each individual gene (Figure 2E, Spearman R = 0.83, *P = 0.01*), suggesting that genes with higher rates of alternative splicing (e.g., *BCL2L11* and *BMF*) are more likely to be sensitive to splicing modulation. E7107 treatment led to the emergence of novel splicing junctions in the coding regions of, among others, *MCL1*, *BMF*, and *BCL2L11* but not within *BCL2*

(Supplemental Figure 3). Across the 11 CLL samples, we detected the skipping of exon 2 within *MCL1* coupled to IR of the flanking introns (introns 1 and 2) (Figure 3A, $P = 0.001$). In addition, we also found the skipping of exon 4 within the main isoform of *BMF* in all 11 CLL samples ($P = 0.001$). In 9 of 11 CLL samples, we observed skipping of exon 3 within the main isoform of *BCL2L11* ($P = 0.0039$). In contrast, the most significantly modulated splice event within *BCL2* was not within its coding region but was a retention of a short intron (189 aa) upstream of the *BCL2*-coding sequence ($P = 0.001$).

All targets in these 4 BCL2 family members could be validated by reverse-transcriptase PCR (RT-PCR) of cDNA preparations from 3 of the 11 CLL samples characterized by RNA-seq (Figure 3B). We observed depletion of the main transcriptional isoform of *MCL1* (*MCL1*$_L$), of *BMF* (variants 1 [v1] and 2 [v2]), and of *BCL2L11* transcripts encoding *BIM*$_{EL}$, *BIM*$_L$, and *BIM*$_s$ and accumulation of lower-molecular-weight products (MCL1 isoform-s [*MCL1s*], *BMF v4* and *BCL2L11 v8*) consistent with exon-skipped transcripts. Accumulation of a transcript consistent with *BCL2L11 v12* could also be detected after E7107 treatment, possibly as a result of alternative 5′ splice site usage within *BIM*$_{EL}$. In contrast, the coding region of *BCL2* was not altered by E7107 treatment. In line with the transcript level findings, we detected stable levels of BCL2 protein but reduced protein expression of MCL1 (i.e., the protein product of the main transcriptional isoform *MCL1*$_L$), of BMF isoforms, and of BIM$_{EL}$ (i.e., the highest-molecular-weight isoform of BIM) in 4 independent CLL samples, following overnight incubation with 3 nM E7107 on NK-TERT stroma, an immortalized human BM-derived cell line used to protect CLL cells from spontaneous apoptosis in culture (20) (Figure 3C). Of note, despite the observed reduction in *BIM*$_L$ transcript levels, BIM$_L$ protein levels were not reduced in the presence of E7107, suggesting higher stability of this isoform in this experimental context. Levels of nucleolin, a *BCL2* mRNA–stabilizing protein known to be overexpressed in CLL (21), were also not altered by E7107 (Figure 3C), possibly contributing to stabilization of productive *BCL2* transcripts.

*Spliceosome modulation increases BCL2 dependence and sensitizes CLL to venetoclax treatment*. Given the transcriptional alterations induced by E7107 to BCL2 family members, we asked how E7107 treatment could perturb mitochondrial apoptotic dependencies in primary CLL cells. To address this question, we used dynamic BH3 profiling (DBP), a functional technique that measures the early net proapoptotic signaling induced after drug treatment as well as changes in cellular dependencies on antiapoptotic proteins for survival (22, 23). We used this approach to analyze 14 CLL patient samples (Supplemental Table 3) after overnight incubation with 3 nM E7107 in the presence of NK-TERT stromal support. After E7107 treatment, we consistently detected increased cytochrome *c* release following incubation with PUMA and BAD BH3 peptides (Figure 4A, $P = 0.0002$ and 0.0001, respectively), suggesting increased overall mitochondrial priming for apoptosis and dependence on BCL2/BCLxL, respectively. Since incubation with the BAD BH3 peptide measures both BCL2 and BCLxL dependence, we also selectively tested BCLxL dependence with the HRK BH3 peptide. We found that E7107 treatment led to minimal change in cytochrome *c* release by HRK, indicating that E7107 selectively increases BCL2 dependence, without affecting BCLxL. These data are consistent with our finding (Figure 2D) and those of a previous report (24) demonstrating that BCLxL is not a target of splicing modulation. Notably, cytochrome *c* release with MS1 peptide exposure was significantly decreased ($P = 0.0002$), whereas no clear change in BFL1 dependence was observed after E7107 treatment. Modulation of apoptotic dependencies was consistent across samples, irrespective of *SF3B1* mutation status ($P < 0.05$ for comparisons of PUMA, BAD, and MS1 BH3 peptides within *SF3B1*$^{wt}$ and *SF3B1*$^{mut}$ samples, Supplemental Figure 4).

Given the increased BCL2 dependence after E7107 treatment, we reasoned that E7107 may enhance sensitivity of CLL cells to the BCL2 inhibitor venetoclax. Based on the E7107 viability analyses (per Figure 1F) and our previous experience with venetoclax in vitro responses (25), we chose concentrations of lower than 10 nM to limit the extent of apoptosis induced by either agent alone. We observed decreased viability in 26 CLL patient samples when treated with the combination of E7107 (1–3 nM) and venetoclax (1 nM) for 8 hours compared with treatment with E7107 or venetoclax alone (Supplemental Table 3; Figure 4B, left; $P = 0.001$ and $P = 0.0004$, respectively). Combination treatment was also able to sensitize cells to apoptosis in the presence of stromal support from NK-TERT (Figure 4B, right; $P = 0.003$ and $P = 0.03$, respectively), as tested on 12 patient samples. BH3 profiling data were available from 8 of these 12 samples and revealed that increased BCL2 dependence after E7107 was associated with increased sensitivity to venetoclax treatment (Figure 4C, Spearman $R = 0.976$, $P < 0.0001$). As a marker of apoptosis induction, we observed increased PARP cleavage in 4 CLL samples and confirmed decreased expression of MCL1 and a lack of marked change of BCL2 protein levels after treatment with E7107 alone or in combination with venetoclax (Figure 4D).

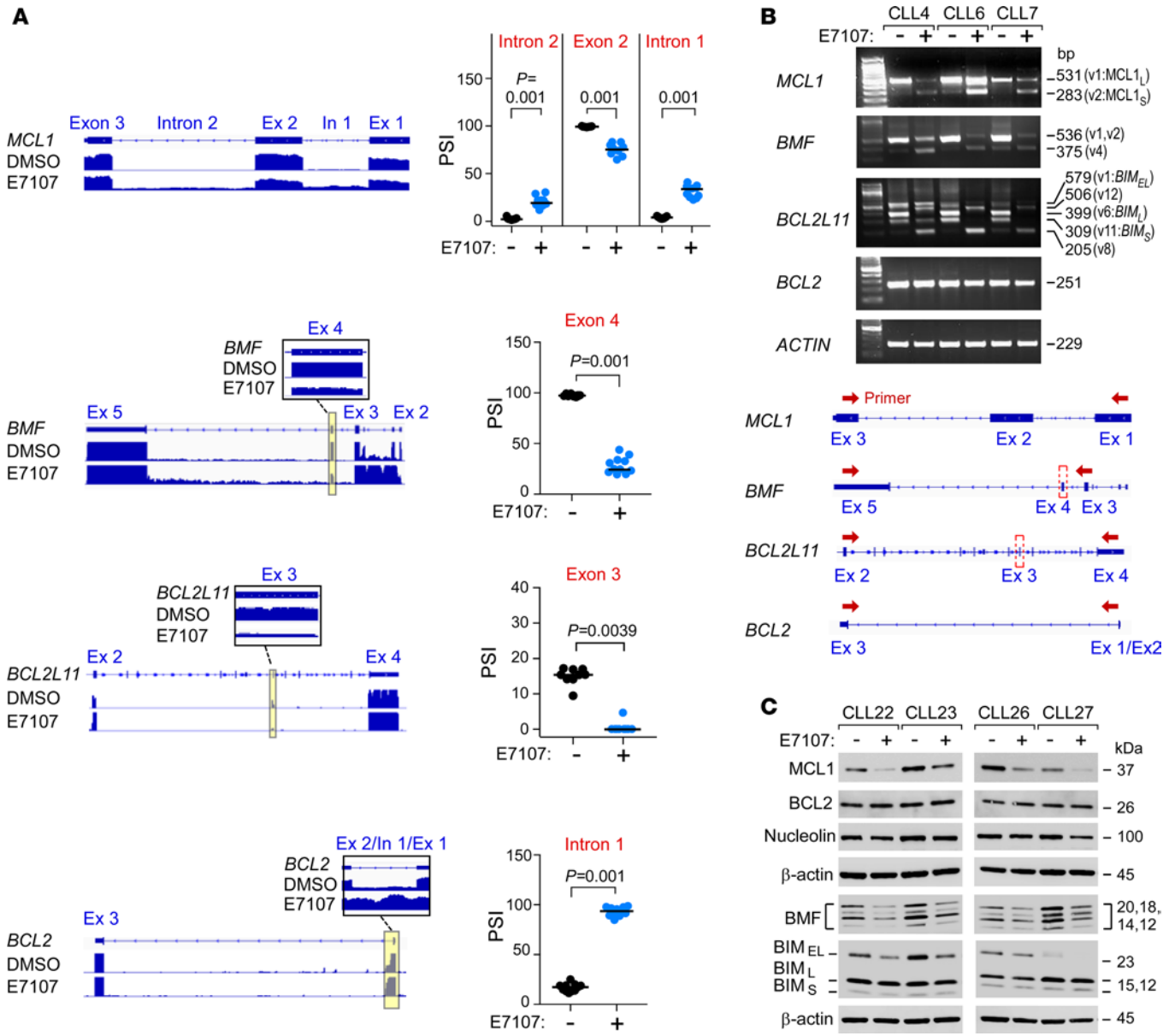


**Figure 3. E7107 differentially targets BCL2 family members.** (**A**) Representative RNA-sequencing tracks of *MCL1*, *BMF*, *BCL2L11*, and *BCL2* genes of 1 sample after 8 hours of treatment with DMSO or 5 nM E7107, and percent spliced in (PSI) values of junction reads within selected intron retention or cassette exon–skipping events (yellow shaded areas) of the 11 analyzed CLL samples. 9 of 11 samples are shown for *BCL2L11*, due to 2 instances of low gene expression within the E7107 treatment group. In, introns; Ex, exon. Reported *P* values were calculated by Wilcoxon signed-rank test. Corresponding Sashimi plot representations are displayed in Supplemental Figure 3. (**B**) RT-PCR of 3 CLL samples (CLL4, CLL6, CLL7) after 8-hour treatment with 5 nM E7107 to assess levels of *MCL1*, *BMF*, *BCL2L11*, and *BCL2*. *ACTIN* is used as internal control. The length of the main amplified isoforms is indicated in base pairs (bp). V, variant. Red arrows indicate primer positioning within each gene, and red dotted lines highlight exon 4 within *BMF* and exon 3 within *BCL2L11*. (**C**) Western blot analysis of MCL1, BCL2, nucleolin, BMF, and BIM isoforms in 4 CLL samples (CLL22, CLL23, CLL26, CLL27) before and after overnight treatment with 3 nM E7107 in the presence of NK-TERT stromal support. β-Actin is used as loading control. Molecular weights (in kDa) are indicated in the figure.

*The Eμ-TCL1 model shows high MCL1 dependence and low venetoclax sensitivity, which can be reverted by E7107.* The Eμ-TCL1 mouse model (26) and its adoptive transfer (27) represent two treatment platforms commonly used for drug testing in CLL. Although these mice were previously described to express BCL2 and MCL1 proteins (28), the apoptotic dependencies of the CLL-like disease generated in this model have not previously been explored. We performed DBP analyses of 7 leukemic splenocyte (SP) preparations from 12-month-old TCL1 mice (Figure 5A) and compared dependencies on the main antiapoptotic factors (i.e., BCL2, MCL1, BCLxL, BFL1) to those of the previously tested 14 primary CLL samples. Whereas BCL2 dependence was not significantly different between TCL1-derived and CLL patient cells, we noted

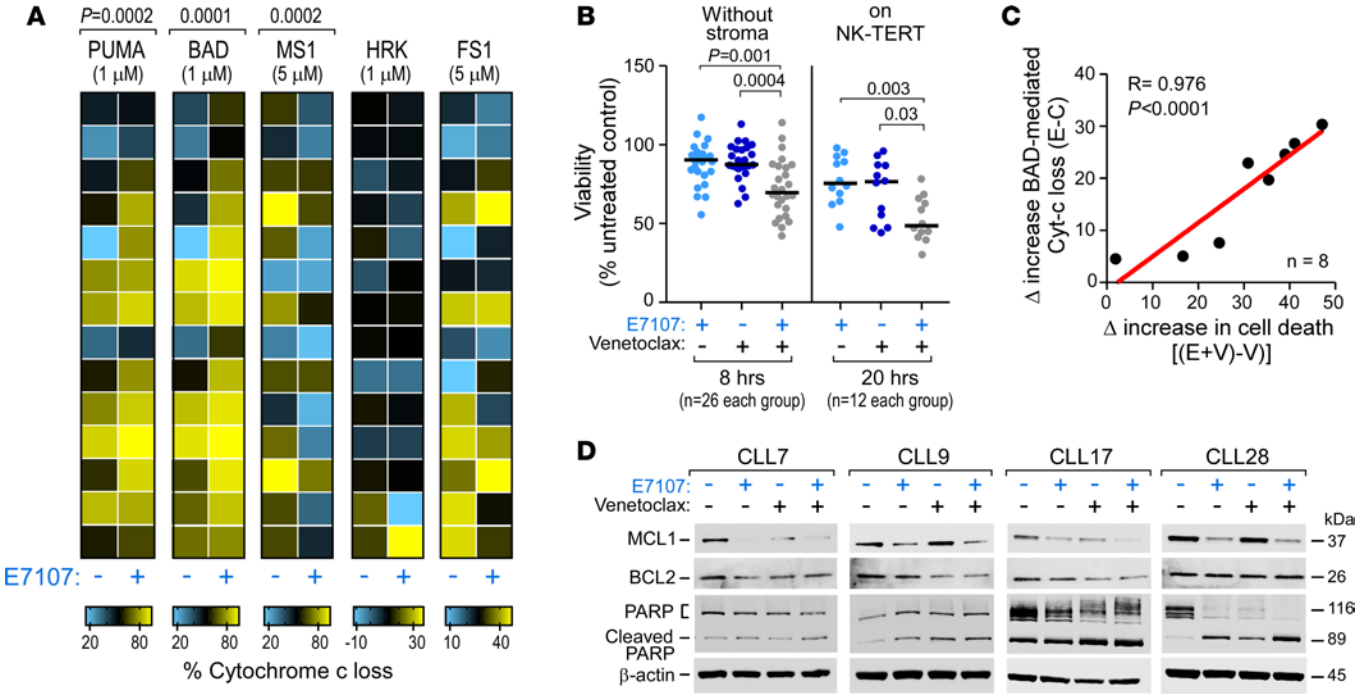


**Figure 4. Splicing modulation sensitizes CLL cells to venetoclax by reducing MCL1 and increasing BCL2 dependence.** (**A**) Heatmap of percentage cytochrome *c* loss, as quantified by flow cytometry on 14 CLL samples after overnight treatment with 3 nM E7107 or DMSO in the presence of NK-TERT stromal support (cyan, lowest value; yellow, highest value). Images from left to right refer to overall priming (PUMA 1 μM), BCL2 dependence (BAD 1 μM), MCL1 dependence (MS1 5 μM), BCLxL dependence (HRK 1 μM), and BFL1 dependence (FS1 5 μM). Reported *P* values were calculated by Wilcoxon signed-rank test. A representation of the data with samples subdivided based on *SF3B1* mutation status is provided in Supplemental Figure 4. (**B**) Normalized viability values as a percentage of the untreated control of 26 CLL samples after 8-hour treatment with 1 nM E7107 and/or 1 nM venetoclax in the absence of stromal support or 20-hour treatment of 12 CLL samples with 3 nM E7107 and/or 1 nM venetoclax in the presence of stromal support by NK-TERT. Reported *P* values were calculated by 1-way ANOVA with Scheffé's correction for multiple comparisons. (**C**) Linear regression of Δ increase in BAD-mediated cytochrome *c* (Cyt-c) loss (*y* axis) and Δ increase in cell death of 8 CLL samples after treatment with E7107 and venetoclax (E+V) as compared with venetoclax treatment alone (V) (*x* axis). Spearman correlation *R* and *P* values are indicated in the figure. (**D**) Western blot analysis of MCL1, BCL2, PARP, and cleaved PARP protein levels before and after treatment with E7107, venetoclax, or the combination of both on 4 CLL samples (CLL7, CLL9, CLL17, CLL28) in the presence of NK-TERT stroma. β-Actin was used as loading control. Treatment conditions were the same as those in **B**. Molecular weights (in kDa) are indicated in the figure.

strikingly increased MCL1 and BFL1 dependence (Figure 5A, $P < 0.0001$ and $P = 0.016$, respectively) in TCL1-derived cells. BCLxL dependence was consistently low across human and murine CLL. Given the potential importance of MCL1 and BFL1 in mediating resistance to venetoclax treatment (29–32), we hypothesized a lower TCL1 SP sensitivity to venetoclax compared with that of human CLL cells. Indeed, we observed a lower reduction in viability of 5 TCL1 SP samples compared with 6 CLL patient samples after overnight incubation with 1 nM and 5 nM venetoclax (Figure 5B, $P = 0.02$ and 0.004, respectively) in the presence of OP9 stroma; some degree in vitro apoptosis of TCL1 cells could be induced by venetoclax treatment (up to 50% for 2 of the cases when treated with 5 nM venetoclax), consistent with the detectable BCL2 dependence of the model, although such viability reduction was strikingly lower than the one of primary CLL samples. The murine line OP9 was chosen as a more suitable stromal support for murine SPs (33) and showed similar protective properties as human NK-TERT for primary CLL samples (Supplemental Figure 5A, $P < 0.05$).

To assess whether E7107 treatment could perturb apoptotic dependencies in TCL1 mice in a fashion similar to primary CLL, we performed DBP of SPs from TCL1 mice after an 8-hour treatment with 5 nM E7107 in the presence of OP9 stroma. Similar to primary CLL samples, we detected increased overall priming ($P$ [PUMA] = 0.03), increased BCL2 dependence ($P$ [BAD] = 0.016), decreased MCL1 dependence ($P$ [MCL1] = 0.016), and unchanged BCLxL dependence after E7107 treatment (Supplemental Figure 5B). In contrast to primary CLL, and possibly linked to the higher baseline BFL1 dependence of TCL1 cells, we also detected increased BFL1 dependence ($P$ [FS1] = 0.016) after E7107 treatment. These shifts were particularly evident when calculating Δ priming values, a measure of the net change in proapoptotic signaling after E7107 treatment compared with the DMSO control (Figure 5C). Increased BCL2 dependence after splicing modulation

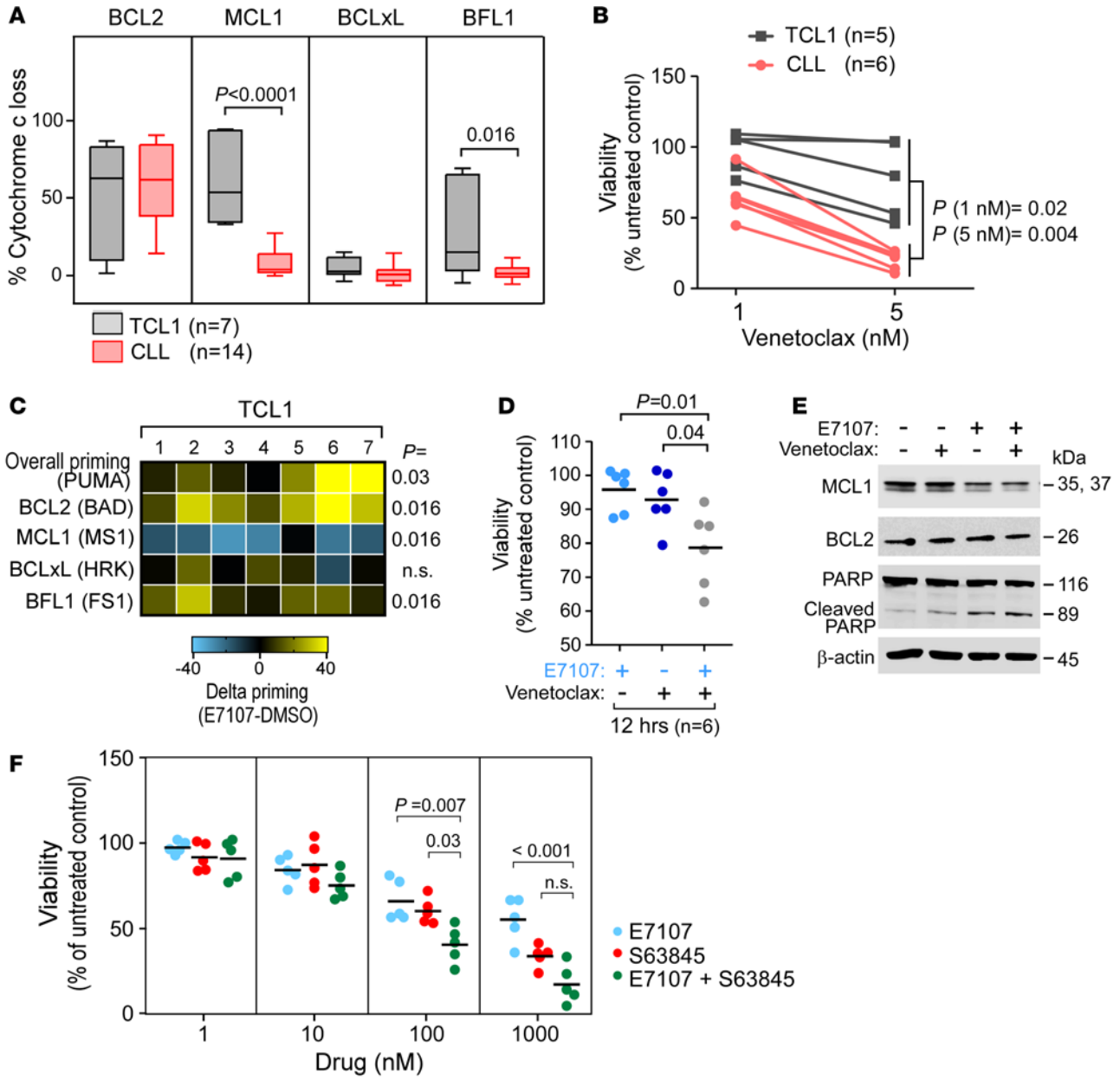


**Figure 5. The Eμ-TCL1 mouse model shows high MCL1 dependence and resistance to venetoclax.** (**A**) Baseline BH3-profiling analysis of 7 TCL1 splenocyte preparations as compared with the previously analyzed 14 CLL samples. Graphs from left to right refer to percentage cytochrome *c* loss after incubation with 1 μM BAD peptide (BCL2 dependence), 1 μM MS1 (MCL1 dependence), 1 μM HRK (BCLxL dependence), and 1 μM FS1 (BFL1 dependence). Reported *P* values were calculated by Mann Whitney *U* test. (**B**) Viability measurement as a percentage of the untreated control of 5 TCL1 splenocyte samples and 6 CLL samples after overnight treatment with 1 nM and 5 nM E7107 on OP9 stroma. *P* values were calculated by Mann Whitney *U* test. (**C**) Heatmap of Δ priming values of 7 TCL1 splenocyte samples after 8-hour treatment with 5 nM E7107 as compared with DMSO-treated controls (cyan, lowest value; yellow, highest value). *P* values of comparisons between E7107 treatment and DMSO were calculated by Wilcoxon signed-rank test. Individual values of DMSO- or E7107-treated samples are displayed in Supplemental Figure 5B. (**D**) Viability measurement as a percentage of the untreated control of 6 samples after overnight treatment with 1 nM E7107, 5 nM venetoclax, or the combination of both on OP9 stroma. Reported *P* values were calculated by 1-way ANOVA with Scheffé's correction for multiple comparisons. (**E**) Western blot analysis of MCL1, BCL2, PARP, and cleaved PARP levels of 1 representative TCL1 sample after overnight treatment with 1 nM E7107, 5 nM venetoclax, or the combination of both. β-Actin was used as loading control. Molecular weights (in kDa) are indicated in the figure. (**F**) Viability measurement as a percentage of the untreated control of 5 TCL1 samples after 8 hours of treatment with increasing concentrations of E7107, S63845, or the combination of both. Reported *P* values were calculated by 1-way ANOVA with Scheffé's correction for multiple comparisons.

sensitized TCL1 cells to venetoclax, as assessed after overnight treatment with 5 nM venetoclax in the presence of 1 nM E7107 (Figure 5D, $P < 0.05$). E7107 and venetoclax drug doses were chosen in this setting based on their similar potency in reducing TCL1 cell viability when tested as single agents (Supplemental Figure 5C). Similar to primary human CLL cells, increased PARP cleavage and decreased MCL1 protein expression were detected after E7107 or E7107 combined with venetoclax, with stable BCL2 expression levels, as shown in one representative TCL1 SP sample (Figure 5E). We observed similar killing profiles when TCL1 SPs from 5 mice were exposed for 8 hours to increasing concentrations of either E7107 or the MCL1 inhibitor S63845 (34), with marked additive activity when both drugs were administered at 100 nM (Figure 5F, $P < 0.05$). Like E7107, 1 nM S63845 reduced SP viability when combined with 5 nM venetoclax overnight on OP9 stroma (Supplemental Figure 5D, $P < 0.05$).

*Splicing modulation sensitizes murine CLL-like cells to venetoclax treatment*. To evaluate the effects of E7107 alone or in combination with venetoclax in vivo, we first evaluated the effects of E7107 alone in 12-month-old TCL1 animals. We selected the dose of 1–2 mg/kg to ensure splicing modulation but absence of apoptosis induction in normal B cells, as tested in C57BL/6J wild-type mice treated for 4 days with a range of doses of E7107 (Supplemental Figure 6A). Minimal, if any, apoptosis of normal T cells was detected at any of the tested doses of E7107 (Supplemental Figure 6B). Across this range of doses, we observed comparable reductions in the levels of mature isoforms of the known targets of E7107 *Slc25a19* and *Dph2* RNAs in cDNA preparations from the peripheral blood (PB) of the treated animals 3 hours after the first E7107 injection, consistent with in vivo splicing inhibition (Supplemental Figure 6, C and D, $P < 0.05$).

To test the short-term effects of E7107 on CLL-like disease, we treated ten 12-month-old TCL1 mice with a disease load ranging from 20% to 70% $B220^+CD5^+Ig\kappa^+$ cells in the PB (Supplemental Figure 7A). Treatment resulted in in vivo splicing inhibition (Supplemental Figure 7B, $P < 0.05$) reduced spleen weight (Supplemental Figure 7C, $P = 0.028$) and reduced $B220^+CD5^+Ig\kappa^+$ CLL cell infiltration of PB and BM compared with control vehicle-treated mice (Supplemental Figure 7, D and E, $P < 0.05$ for PB and BM comparisons). Despite the observed reduction in spleen weight, the overall reduction in percentage of $B220^+CD5^+Ig\kappa^+$ CLL infiltration in the spleen was not statistically significant ($P = 0.15$) and was also minimal in the peritoneal cavity (PC), possibly due to the high disease burden of these animals. Treatment was well tolerated, as body weight loss was less than or equal to 10% throughout the 5-day treatment window (Supplemental Figure 7F). Likewise, adoptive transfer of Eμ-TCL1 SP cells into 16 CD45.1 recipients, allowing for induction of disease with similar kinetics across a large number of recipients and thereby limiting experimental heterogeneity (Figure 6A), revealed marked reductions in SP dimension and weight (Figure 6B, $P = 0.007$) as well as disease burden in the PB, SP, PC, and BM of the treated animals (Figure 6C, $P < 0.05$ for all comparisons) at the end of treatment. Decreased protein levels of MCL1 were detected in SP preparations from 3 mice per group at the end of treatment (Figure 6D), confirming this protein as a target of E7107 in vivo.

To examine the effects of combination treatment of E7107 with venetoclax in vivo, we transplanted Eμ-TCL1 SPs into 28 additional CD45.1 animals and treated them for 2 weeks with 1 mg/kg E7107 and/or 100 mg/kg venetoclax (7 mice/group). Venetoclax dosing was chosen based on previously reported efficacy and safety profiles in xenograft lymphoma models (35), while E7107 was lowered to 1 mg/kg to reduce its potency as single agent. Treatment was well tolerated throughout the 2-week treatment window (Supplemental Figure 8A), and the superior effect of the combination treatment over single agents in reducing SP dimension, weight, and the percentage of infiltrating $B220^+CD5^+Ig\kappa^+$ CLL cells could be readily appreciated at the end of treatment (Figure 6, E and F, $P < 0.05$). Combination treatment also reduced disease burden in the PB, PC, and BM (Supplemental Figure 8B, $P \leq 0.008$), although not to a significantly greater extent than single-agent E7107 in these organs, which may, at least for PC and BM, be explained by the particularly high MCL1 dependence of CLL cells in these tissues (Supplemental Figure 8C). In line with this, differences in MCL1 dependencies, but not in BCL2, BCLxL, or BFL1, were detected in the BH3 profiles of paired organs in 5 independent TCL1 mice in the absence of any drug treatment (2-way ANOVA, $P$ [MCL1] = 0.001). The effects in the PB may be, at least partly, related to greater drug bioavailability with intravenous administration of E7107. Animals treated with venetoclax monotherapy, as well as vehicle controls, displayed a lack of leukemia elimination from the SP after 2 weeks of treatment, and immunohistochemical analyses revealed a largely disrupted splenic architecture, with marked infiltration of cells staining positive for the proliferation marker Ki67 and coexpressing CD5 and PAX5 (Figure 6G), particularly in the proximity of T cell–rich zones. Such infiltration was reduced after treatment with single-agent E7107, and this change was even more evident after combination treatment,

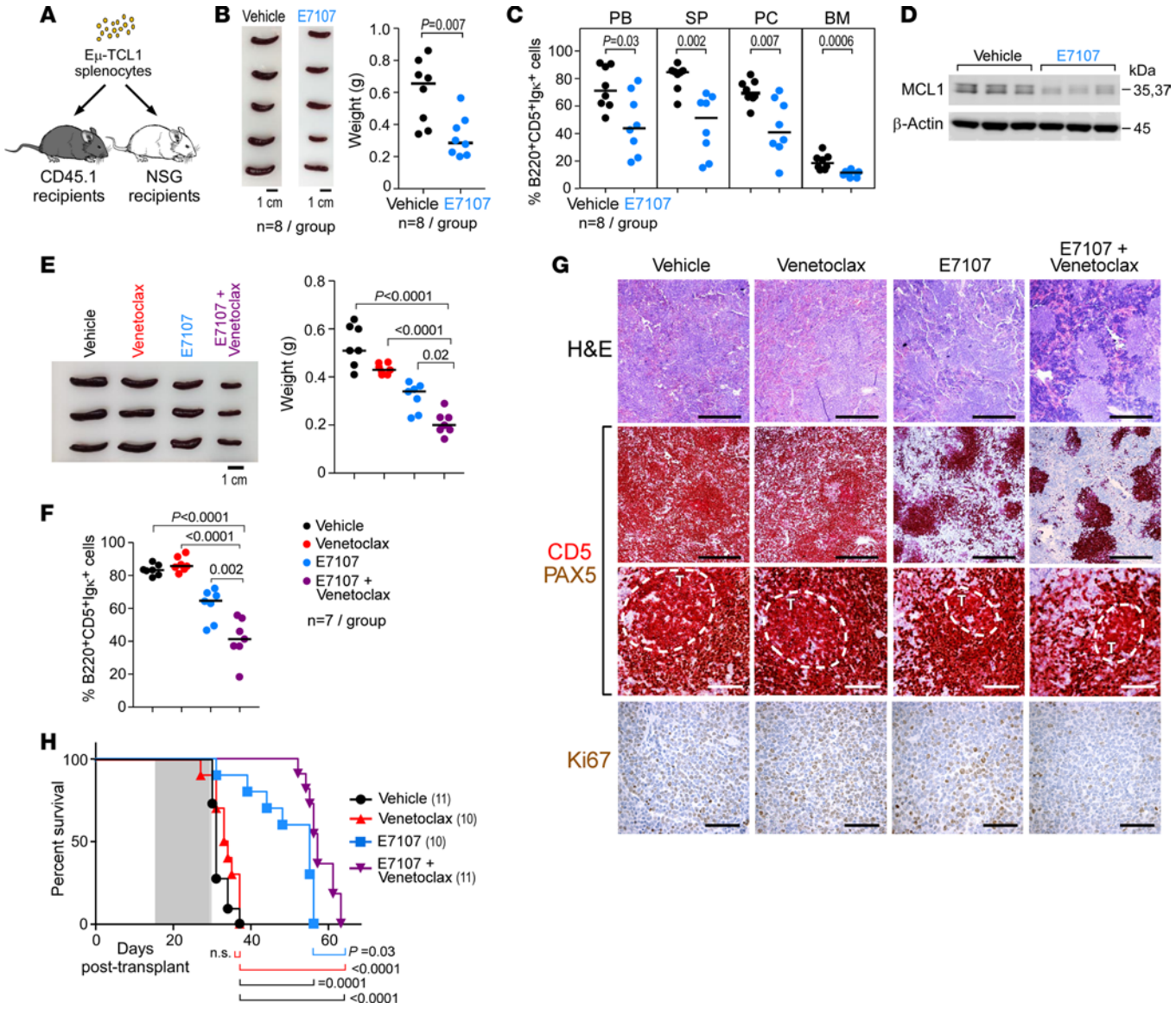


**Figure 6. Splicing modulation overcomes venetoclax resistance in vivo in the Eμ-TCL1–based transplant model of CLL.** (**A**) Schema of adoptive transfer of Eμ-TCL1–derived splenocytes into immunocompetent CD45.1 or immunodeficient NSG recipients. (**B**) Representative spleens of 5 vehicle control-treated and 5 E7107-treated animals, as harvested at the end of treatment. Scale bar: 1 cm. *P* value was calculated by Mann Whitney *U* test. (**C**) Flow cytometry analysis of peripheral blood (PB), spleen (SP), peritoneum (PC), and bone marrow (BM) to measure the percentage of B220$^+$CD5$^+$Igκ$^+$ CLL cells from mice treated with vehicle control or with 2 mg/kg E7107. *P* values were calculated by Mann Whitney *U* test. (**D**) Western blot analysis of MCL1 protein levels in the splenocytes of 3 CD45.1 animals/group, as analyzed at the end of treatment with 2 mg/kg E7107. β-Actin is used as loading control. Molecular weights (in kDa) are indicated. (**E**) Representative spleens of 3 CD45.1 mice per group treated with vehicle control, single-agent 100 mg/kg venetoclax, single-agent 1 mg/kg E7107, or the combination of both, as harvested at the end of treatment (*n* = 7/group). Scale bar: 1 cm. Reported *P* values were calculated by 1-way ANOVA with Scheffé's correction for multiple comparisons. (**F**) Flow cytometry analysis of the percentage of B220$^+$CD5$^+$Igκ$^+$ CLL cells in spleens from mice belonging to the 4 treatment groups, as analyzed at the end of treatment. Reported *P* values were calculated by 1-way ANOVA with Scheffé's correction. (**G**) Representative spleen sections (1 mouse/group) of CD45.1 transplants stained with H&E, anti-PAX5 (brown), and anti-CD5 (red) antibodies or anti-Ki67 at the end of a 2-week treatment with E7107 or venetoclax alone or in combination, as indicated in the figure. White dotted lines demarcate CD5$^+$PAX5$^-$ T cell areas. The CLL infiltrate is composed of cells coexpressing cytoplasmic CD5 and nuclear PAX5. The first and second rows display images captured using a ×5 objective (scale bar: 1 cm), the third and fourth display images captured using a ×40 objective (scale bar: 100 μM). (**H**) Survival curve of NSG mice transplanted with TCL1 splenocytes and then treated with vehicle control (*n* = 11), 25–50 mg/kg venetoclax (*n* = 10), 2 mg/kg E7107 (*n* = 10), or the combination of venetoclax and E7107 (*n* = 11) for 2 weeks, followed by observation for survival. *P* values were calculated using the log-rank test with Bonferroni correction. The gray shaded area indicates treatment period.

which also restored normal splenic architecture. To observe the longer-term effects of E7107 alone or in combination with venetoclax, we performed adoptive transfer of Eμ-TCL1 SPs into 42 immunodeficient NSG animals (Figure 6A). After 2 weeks of treatment with 2 mg/kg E7107 and 25–50 mg/kg venetoclax, the latter escalated in a schedule similar to the human clinical setting to reduce the risk of tumor lysis syndrome (1) in this faster progression model, the animals were observed over 1 month for survival (Figure 6H). In addition to a pronounced increase in overall survival after treatment with single-agent E7107 compared with treatment with either vehicle control or single-agent venetoclax ($P \leq 0.0001$), we also observed increased overall survival of animals treated with the combination of E7107 and venetoclax, as compared with treatment with single-agent E7107 (Figure 6H, $P = 0.03$). The venetoclax treatment group had a similar life span to that of control-treated animals ($P = 0.67$), confirming the minimal sensitivity of this model to venetoclax treatment alone.

## Discussion

Alternative splicing is a tightly regulated process, which is frequently aberrant in cancer, and accumulation of aberrantly spliced products is associated with drug resistance mechanisms (36). Splicing modulators are a novel class of therapeutics and include spliceostatin, pladienolide and its derivatives, and the sudemycins (37, 38). These agents are all natural derivatives of different strains of bacteria that share the common mechanisms of action of interfering with the proper assembly of the spliceosome onto a newly transcribed pre-mRNA. Altogether, these agents generally induce widespread IR (39), which may result in altered transcriptional products, leading to truncated or inactive proteins (40). In myeloid malignancies, the use of splicing modulators has been associated with selective killing of cells carrying spliceosome mutations (41, 42). In CLL, however, splicing modulators, including spliceostatin (24), sudemycins (43) and pladienolide and its derivatives (44, 45), display cytotoxicity to leukemic lymphocytes irrespective of *SF3B1* mutation status, while sparing normal B cells. Our work provides evidence of a vast difference, both quantitatively and qualitatively, between the extent of splicing aberrations and types of transcripts affected in CLL cells as compared with normal B cells. In contrast to the widespread IR observed in most tumors (46), we found intronic splicing as a characteristic of CLL cells compared with normal B cells, suggesting it as a mechanism of gene expression regulation adopted by CLL cells to facilitate productive transcription of selected gene targets. At least in this mature B cell malignancy, while there are clear aberrations associated with mutation of *SF3B1*, we also observed splicing alterations characteristic of the malignant cells irrespective of splicing factor mutation that affect numerous CLL survival pathways. This finding provides an explanation for the sensitivity of CLL to splicing modulation regardless of *SF3B1* mutation status.

These results pave the way for an exploration of how we can take advantage of this biology for therapeutic purpose. In particular, we indicate that the tool compound E7107 affects the apoptotic pathway but also can shift apoptotic dependencies by reducing MCL1 dependence while favoring BCL2 dependence, providing the therapeutic opportunity for combination treatment with BCL2 inhibitors. Consistently, combining splicing modulation with venetoclax sensitized both human and murine CLL cells to venetoclax treatment in vitro, and overcame venetoclax treatment resistance in vivo, in mouse models of CLL-like disease. In line with our findings, combination of venetoclax and the splicing modulator spliceostatin was previously shown to overcome IL-4 and CD40 ligand prosurvival signals in primary CLL (24).

In addition, we here report on an unexpectedly high MCL1 dependence of the TCL1 model, which was associated with limited sensitivity to venetoclax treatment in vitro and in vivo. Our findings are in line with a recent study reporting on the limited efficacy of venetoclax when administered in vivo to TCL1 transplants (47). Both studies support the usefulness of the TCL1 model system for investigating venetoclax treatment resistance. At the same time, our collective results challenge the suitability of this mouse model as a faithful platform for studies of the pathophysiology of a predominantly BCL2-dependent human malignancy.

"Mitochondrial remodeling," considered to be the reprogramming of mitochondrial apoptotic dependencies after drug exposure, in the context of BCL2-dependent malignancies, such as CLL (48, 49), can therefore be conceivably exploited in cases of limited sensitivity or resistance to BCL2 inhibition (Figure 7). Although the clinical applicability of the tool compound E7107 has been challenged by dose-limiting toxicities (50), its structural and functional similarity to the other members of this class of compounds provide insight on a more general mechanism of action of these drugs. The broad range of pathways targeted by these agents may provide opportunities for combinatorial treatment strategies with other targeted therapies, including B cell receptor signaling inhibitors, as proposed by a previous report (43). Considering

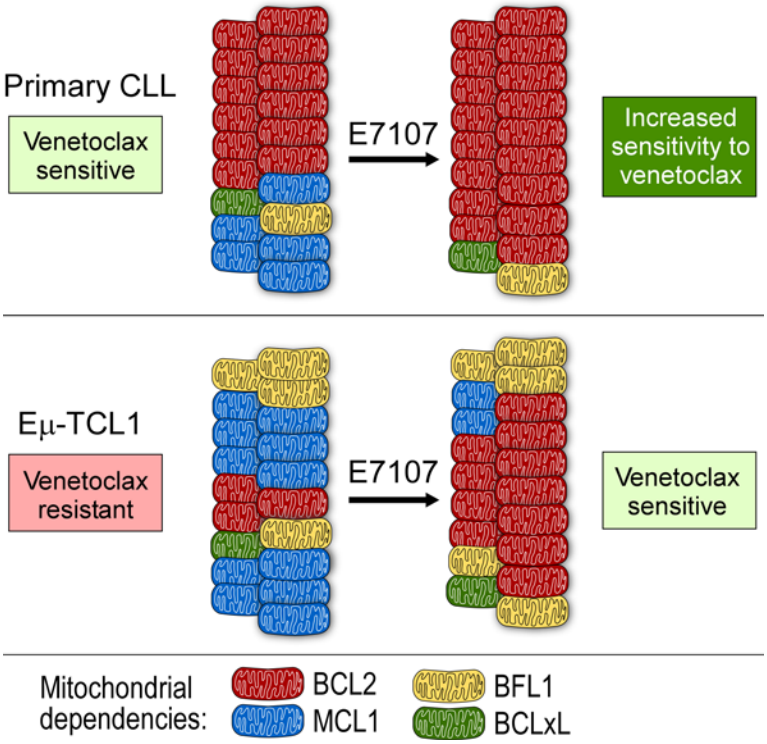


**Figure 7. Schematic representation of the "mitochondrial remodeling model."** The splicing modulator E7107 redirects apoptotic dependencies in CLL. In the context of primary CLL, BCL2 dependence and venetoclax sensitivity can be increased following splicing modulation by E7107. In the context of a venetoclax-resistant model, such as the TCL1 mouse, MCL1 dependence contributes to venetoclax resistance and can be targeted by E7107 treatment, favoring venetoclax sensitivity. Mitochondrial antiapoptotic dependencies before and after E7107 treatment of CLL or TCL1 cells are highlighted (red, BCL2; blue, MCL1; yellow, BFL1; green, BCLxL).

the emerging importance of aberrant splicing as a common characteristic of a large number of solid and hematologic tumors (36), our findings also suggest the potential applicability of splicing modulators to a larger number of cancers, including cases in which aberrant splicing is not exclusively driven by the presence of mutations in spliceosome components.

## Methods

*Primary samples and cell lines*. PB mononuclear cells (PBMCs) were isolated from whole blood by density gradient centrifugation over Ficoll-Paque (GE Healthcare) and viably frozen in FBS supplemented with 10% DMSO until the time of analysis. Upon thawing, cells were cultured at $10^7$ cells/ml in RPMI 1640 medium supplemented with 10% FBS (Gibco), 100 U/ml penicillin, and 100 μg/ml streptomycin (Gibco) (complete RPMI). $CD19^+$ $CD5^+$ cells generally accounted for >85%, as measured by flow cytometry. Most samples were utilized in more than one functional assay, as indicated in Supplemental Table 3. The NK-TERT human stromal cell line (Riken Cell Bank) was maintained in complete RPMI; the OP9 murine stromal line was cultured in Minimum Essential Medium-α (MilliporeSigma) supplemented with 100 U/ml penicillin, 100 μg/ml streptomycin, and 100X Glutamax (Gibco).

*Mouse models and strains*. Eμ-TCL1 mice (26) on a C57BL/6J background were a gift of George Widhopf (University of California, San Diego); CD45.1 (B6.SJL-*Ptprc*$^a$ *Pepc*$^b$/BoyJ) and NSG mice (NOD.Cg-*Prkdcscid Il2rgtm1Wjl/SzJ*) were purchased from The Jackson Laboratory.

*Drug treatment and viability analyses*. For in vitro testing of the splicing modulator E7107 (H3 Biomedicine Inc.), the BCL2 inhibitor venetoclax (LC Laboratories) and the MCL1 inhibitor S63845 (Selleckchem) were resuspended in DMSO and stored at –20°C. For in vivo testing, E7107 was resuspended in 10% ethanol and 5% Tween-80 in sterile saline, sonicated for 3 minutes, and administered to animals by intravenous injection; venetoclax was resuspended in 60% phosal 50 propylene glycol, 30% polyethylene glycol 400, and 10% ethanol (35) and administered to animals by oral gavage. Cell viability after drug treatment of viably cryopreserved normal human PBMCs, primary CLL cells, or Eμ-TCL1 SPs was determined by flow cytometric analysis of Annexin V-FITC (BD Pharmingen) and Propidium Iodide (Biolegend) staining and being read on a BD FACS Fortessa machine. Normal B cell viability after treatment of human PBMCs was evaluated on gated $CD19^+$ cells. Flow cytometry data were analyzed by Flowjo version 10.2 (Tree Star Inc.).

*Immunoblotting*. Immunoblotting was performed as previously described (51). Primary CLL and TCL1 cells were incubated on stroma (i.e., NK-TERT and OP9, respectively) and treated with low concentrations

of E7107 (3 nM for CLL, 1 nM for TCL1) and venetoclax (1 nM for CLL, 5 nM for TCL1) to reduce confounding effects of cellular apoptosis. TCL1 cells derived from SPs at the end of the in vivo treatment were lysed immediately, without prior incubation on stroma. Cells were lysed on ice for 15 minutes in RIPA Buffer (MilliporeSigma) containing fresh phosphatase inhibitor cocktail (phosSTOP; Roche-Genentech) and complete protease inhibitor cocktail (Roche-Genentech). Cells were then centrifuged at 16,000 *g* for 15 minutes at 4°C, and supernatants were collected and stored at –80°C until further use. Protein content was determined using the BCA protein assay kit (Thermo Fisher Scientific), according to the manufacturer's instructions. Twenty micrograms of total protein were supplemented with NuPage Sample Buffer (4×) and NuPage Sample Reducing Agent (10×), loaded onto 4%–12% sodium dodecyl sulfate–polyacrylamide gradient gels (Invitrogen), and then transferred to nitrocellulose membranes (Thermo Fisher Scientific). Membranes were blocked for 15 minutes in PBS-Tween containing 5% bovine serum albumin and incubated overnight with primary antibodies (diluted 1:1,000), followed by species-specific HRP-conjugated secondary antibodies (diluted 1:5,000) for 1 hour. Membranes were probed with the following primary antibodies: anti-BCL2 (human specific) rabbit antibody, anti-BCL2 rabbit monoclonal antibody (mAb, mouse preferred, clone C17C4), anti-MCL1 rabbit mAb (clone D35A5), anti-BIM rabbit mAb (clone C34C5), anti-nucleolin rabbit mAb (clone D4C70), anti-PARP rabbit mAb (clone 46D11), and anti–β-actin rabbit mAb HRP conjugated (clone 13E5), all purchased from Cell Signaling Technology, and mouse anti-BMF (clone 6F3), purchased from Novus Biologicals. SuperSignal West Pico Chemiluminescent Substrate (Thermo Fisher Scientific) was used to visualize immunoreactive bands by an LAS 4000 imager (Fuji Film).

*BH3 profiling*. BH3 profiling was performed as previously described (23). Primary CLL cells and freshly harvested Eμ-TCL1 SPs were cultured in complete RPMI and cocultured with the human stroma NK-TERT cell line or OP9 murine stromal cell line (10:1 ratio) in 6-well plates and treated ex vivo with E7107 or DMSO. Cells were removed from the stromal layer for analysis by gentle pipetting. BH3 profiling across tissue compartments (PB, SP, PC, BM) was performed on paired freshly harvested organs from five 10- to 12-month-old Eμ-TCL1 mice, without prior incubation on OP9. Prior to analysis both primary CLL samples and TCL1 cells were suspended in MEB2P buffer (150 mM mannitol, 10 mM HEPES-KOH pH 7.5, 150 mM KCI, 1 mM EGTA, 1 mM EDTA, 0.1% BSA, 5 mM succinate, 0.25% poloxamer 188). Single-cell suspensions were added to 384-well plates and incubated for 60 minutes with 1–5 μM BH3-only peptides (PUMA, BAD, MS1, HRK and FS1) combined with either 0.002% digitonin for permeabilization of primary CLL cells or 0.003% digitonin for Eμ-TCL1 SPs. After fixation with 4% paraformaldehyde and neutralization with N2 buffer (1.7 M Tris, 1.25 M glycine pH 9.1), cells were stained overnight with a cocktail of anti–cytochrome *c*–Alexa Fluor 488 (6H2.B4/612308, Biolegend), anti–CD19-PE/Cy7 (anti-human [H13B19/302216], BioLegend; anti-murine [ID3/552854], Thermo Fischer Scientific), anti–CD5-PE (anti-human [UCHT2/300608], Biolegend; anti-murine [53-7 3/553023], Thermo Fischer Scientific), and Hoechst 33342 (H3570, Invitrogen) and analyzed using a BD FACS Fortessa. Flow cytometry data were analyzed using FACS Diva version 8.0.1 (BD Pharmingen). Individual analyses were generally performed in triplicate for all drug treatment conditions. Cytochrome *c* release was used to assess the degree of mitochondrial outer membrane permeabilization in response to each BH3 peptide, which was normalized relative to cytochrome *c* release with DMSO (0% loss, negative control) and the ion-channel forming peptide alamethicin (100% loss, positive control). BAD peptide was used as measure for BCL2 and BCLxL dependence, MS1 peptide for MCL1 (52), HRK peptide for BCLxL (53), and FS1 peptide for BFL1 (54). The PUMA peptide, which interacts promiscuously with all of antiapoptotic proteins, served as a marker of overall mitochondrial priming for apoptosis.

*RNA-seq and pathway analysis*. RNA-seq was performed as previously described (10). Briefly, total RNA was extracted from primary CLL cells after an 8-hour treatment with either DMSO or 5 nM E7107 using the RNAeasy Mini Kit (Qiagen) and assessed for quality and quantity (RNA 6000 Nano LabChip kit on a 2100 Bioanalyzer, both from Agilent). Poly-A–selected RNA-Seq libraries were prepared according to standard Illumina protocols. cDNA libraries were checked for quality and quantified using the DNA-1,000 kit (Agilent) on a 2100 Bioanalyzer. Each library was sequenced with the Illumina Sequencing Kit v4 on one lane of a Gene Analyzer IIX sequencer to obtain 76 base-paired end reads. Libraries were pooled and sequenced on a HiSeq2000 (Illumina) to obtain 101 base-paired end reads. Splicing patterns were analyzed using the JuncBASE algorithm (15). The top 200 most variable splicing events within normal B cells and within all CLL samples were identified as events with the highest median absolute deviation in PSI compared with the median PSI for each individual event. For differential splicing

analyses, we selected splicing events with a Benjamini-Hochberg FDR <10% and a difference in |PSI| >10% between the median values of normal B and CLL samples or E7107-treated versus DMSO-treated samples as our most confident set of splicing changes. For the most variable splicing and for differential splicing analysis, at least 2–3 of the samples in each group had to have sufficient coverage of the splice event for quantification (total normalized read count >10). To identify altered splicing in individual samples, an outlier approach was used. For each splicing event, the top tenth percentile (2-sided) PSI values across normal B cells and CLL cells were considered outlier events. Additionally, the difference in PSI value of the outlier splicing events and the median PSI was >10%. Thresholds were chosen for consistency with those used in the differential splicing analysis. Splicing event outliers were collapsed to a gene level, where a gene was an outlier in a given sample if any of the splicing events of that gene in that sample was an outlier. A binary table was generated (0, no outlier events; 1, presence of splicing outlier) and the total number of splicing outliers per sample was calculated. To analyze the effects of E7107 on individual BCL2 family members, we used a difference in |PSI| >20% to enrich for selected splicing targets. Manual inspection of RNA-seq tracks was performed to detect IR and cassette exon-skipping events, and Sashimi plot representations with a minimum junction coverage set to 50 were obtained by Integrative Genomics Viewer (IGV version 2.3) analysis. The Ensembl genome browser was used for intron and exon annotations. Pathway analysis was performed through the Panther algorithm (16). RNA-seq data were deposited in the database of Genotypes and Phenotypes under accession numbers phs000435.v2.p1 (normal B and CLL samples from Wang et al., ref. 10) and phs001431.v1.p1 (CLL samples treated with E7107).

*In vivo treatment studies*. Dose range-finding studies were conducted on C57BL/6J wild-type mice (3–4 per group), which received doses of 1–4 mg/kg E7107 daily for 4 days by intravenous injection. At the end of treatment, organs were harvested and analyzed by flow cytometry for the percentage of normal B ($B220^+$) or normal T ($CD3^+$) cells that stained positive for Annexin V, used as a marker of cellular apoptosis. Single-agent E7107 was first tested in a cohort of 12-month-old Eμ-TCL1 animals, randomized based on the percentage of $B220^+CD5^+Ig\kappa^+$ detected in the PB by flow cytometry. Animals were treated intravenously for 5 days with 2 mg/kg E7107, and disease burden was measured at sacrifice (1 day after the last dose) by flow cytometry analysis of PB, SP, PC, and BM. SP weight was also recorded. Body weight was monitored daily. The subsequent treatment studies were performed on 8- to 12-week-old CD45.1 mice (preconditioned with 400 rads split dose irradiation) or NSG mice transplanted intravenously with viably cryopreserved SPs from 10- to 12-month-old leukemic Eμ-TCL1 animals. CLL burden in the SP preparation was verified before injection by flow cytometry staining of $B220^+CD5^+Ig\kappa^+$ cells, which were always detected to be >80%. Ten million cells/recipient were resuspended in 100 microliters PBS and injected intravenously into recipient animals. CLL burden in the PB of the transplanted recipients was analyzed weekly starting 2 weeks after transplant by flow cytometry, and treatment was initiated when 30%–40% CLL cells were detectable in the PB. Animals were randomized based on the percentage of $B220^+CD5^+Ig\kappa^+$ cells before being assigned to treatment groups. All treatments were performed for 2 weeks on a 5-days-on/2-days-off treatment schedule. In E7107 single-agent treatment studies, 2 mg/kg E7107 was administered daily by intravenous injection, and disease burden in PB, SP, BM, and PC was evaluated by flow cytometry 1 day after the last dose. In E7107 combination treatment studies with venetoclax, CD45.1 animals were randomized according to the same criteria and treated intravenously with 1 mg/kg E7107 or by oral gavage of 100 mg/kg venetoclax; NSG animals were treated with 2 mg/kg E7107 and 25–50 mg/kg venetoclax (dose escalated from week 1 to week 2). Disease burden in PB, SP, BM, and PC was evaluated by flow cytometry 1 day after the last dose for CD45.1. NSG mice were observed for survival; criteria for euthanasia included hunched posture, difficulties breathing or moving, visible hepatosplenomegaly, and weight loss equal to 15% body weight. Disease burden was verified by flow cytometry in the organs (PB, SP, PC, BM) of the euthanized animals and was detected to be >80% in PB, SP, and PC and >40% in BM.

*RT-PCR*. For validation of E7107 targets, RNA was extracted from 3 CLL samples by the RNAeasy Mini Kit, followed by reverse transcription with SuperScript II Reverse Transcriptase (Thermo Fisher Scientific). The following primers were used to perform a 35-cycle PCR with 1 minute of annealing at 60°C and a 2-minute extension at 72°C: *MCL1* forward: 5′-GAGGAGGAGGAGGACGAGTT-3′; *MCL1* reverse, 5′-ACCAGCTCCTACTCCAGCAA-3′(55); *BCL2* forward, 5′-ATGTGTGTGGAGAG-CGTCAA-3′; *BCL2* reverse, 5′-CACTTGTGGCCCAGATAGG-3′ (12); *BMF* forward, 5′-ATCTCAGT-

GTGTGGAGGAGCTG-3′; *BMF* reverse, 5′-CTGCCCCGTTCCTGTTCTCTTC-3′(13); *BCL2L11* forward, 5′-ATGGCAAAGCAACCTTCTGAT-3′; *BCL2L11* reverse, 5′-CAGGCGGACAATGTAACGTAA-3′(13); *ACTIN* forward, 5′-AGGCCCAGAGCAAGAGAGG-3′; *ACTIN* reverse, 5′-TACATGGCTGGGGTGTTGAA-3′. Primer binding to annotated splice variants was verified by Primer Blast. For validation of splicing inhibition in vivo, PB was drawn through the submandibular vein of animals treated with E7107 3 hours after the first intravenous dose. Red blood cells were lysed by incubation with ACK lysis buffer (Gibco) for 5 minutes at room temperature, washed once in PBS, resuspended in TRIzol Reagent (Ambion), and stored at –80°C until further use. To extract RNA, 200 μl chloroform was added to the TRIzol preparation, incubated for 3 minutes at room temperature, and then spun at 16,000 *g* for 15 minutes to remove the upper phase–containing nucleic acids, out of which RNA was extracted by RNAeasy Mini Kit. Real-time PCR was performed on retrotranscribed cDNA, with the following primers and FAM-conjugated probes (all purchased from Thermo Fisher Scientific): *Dph2* pre-mRNA, forward 5′-ACAGCTTATGGCAGGTATGG-3′; reverse 5′-CTAGGAATTCACTGTGACTGAGG-3′; probe 5′-AGTGACCGTGTTTGCACGATGAGA-3′; *Dph2* mature-RNA, forward 5′-CCCTGACCAGTTACTAGGAGAT-3′; reverse 5′-ACACAGCAGCTGCCATAAG-3′; probe 5′-TTAGCTCCTGTGACTTCCTCCAGC-3′; *Slc25a19* mature-RNA probe (Mm00452682_m1). A *Gapdh*-FAM–conjugated probe (Thermo Fisher Scientific) was used for normalization purposes.

*Immunohistochemistry*. Four-micron-thick sections of formalin-fixed spleen tissues were stained with H&E, according to standard protocols (56); coimmunostained for PAX5 and CD5 expression, according to previously described methods (RD Carrasco, personal communication); or stained for Ki67 expression (57). Anti-PAX5 rabbit monoclonal antibody (clone D7H5X, used at 1:75 dilution) was purchased from Cell Signaling Technology, anti-CD5 rabbit polyclonal antibody (used at 1:300) was purchased from Sino Biological, and anti-Ki67 rabbit polyclonal antibody (used at 1:1,000) was purchased from Vector Laboratories. Histological micrographs were taken using a Leica DM200 microscope and a SPOT Insight QE Model camera with SPOT Advanced acquisition software (Diagnostic Instruments).

*Statistics*. Welch 2-tailed *t* test with Bonferroni correction was used for Figure 1D. Spearman correlation was used to assess linear association in Figure 2E and Figure 4C. Wilcoxon signed-rank test was used for the paired analyses in Figure 3A, Figure 4A, Supplemental Figure 4, and Supplemental Figure 5B. Mann Whitney *U* test was used for Figure 1C; Figure 5, A and B; Figure 6, B and C; Supplemental Figure 6, C (right) and D (right); and Supplemental Figure 7, B, C, and E. One-way ANOVA with Scheffé's correction for multiple comparisons was used for Figure 1F; Figure 4B; Figure 5, D and F; Figure 6, E and F; Supplemental Figure 5, A and D; Supplemental Figure 6, C (left) and D (left); and Supplemental Figure 8B. The log-rank test with Bonferroni correction for multiple comparisons was used for the survival analyses in Figure 6H. Two-way ANOVA was used in Supplemental Figure 8C. *P* values lower than 0.05 were considered as statistically significant.

*Study approval*. PB samples were obtained from patients fulfilling diagnostic and immunophenotypic criteria for CLL at the Leukemia Department at the University of Texas MD Anderson Cancer Center and the Moores Cancer Center at University of California, San Diego, after informed consent and institutional review board approval. Mice were housed and treated at the Dana-Farber Cancer Institute with the approval of the institutional animal care and use committee.

## Author contributions

ETH and CJW designed the study; ETH performed most of the in vitro and in vivo experiments and contributed to the RNA-seq data analysis; RV and JD performed and interpreted human and mouse BH3 profiling analyses, under the supervision of AL and MSD; FFDR, ALG, and PB contributed to the in vivo experiments; JS, SY, MG, JW, MS, PS, L. Wang, RR, ANB, and MLM performed the RNA-seq analyses; L. Werner and DN performed biostatistical analyses and contributed to the study design; MZ and RDC performed immunohistochemical analysis of mouse tissues; MT and SB provided critical reagents and contributed to the design of the in vivo studies; EMG, EK, LZR, JAB, and TJK provided CLL patients samples and clinical annotations; CJW supervised the study overall; and ETH and CJW wrote the manuscript, with contributions from all coauthors.

## Acknowledgments

The authors thank Z. Cartun, K. Baranowski, the Dana-Farber Cancer Institute animal research facility technical team for excellent technical support, and M. Hernandez-Sanchez for helpful suggestions. This study was supported by a grant from the NIH/National Cancer Institute (NIH/NCI) (P01 CA206978) and the NIH/NCI CLL Research Consortium Grant (P01-CA081534). CJW acknowledges support from the NIH/NCI (R01 CA216273, U10 CA180861) and is a scholar of the Leukemia and Lymphoma Society. ETH is a special fellow of the Leukemia and Lymphoma Society.

Address correspondence to: Catherine J. Wu, Dana-Farber Cancer Institute, Dana 520C, 450 Brookline Avenue, Boston, Massachusetts 02215, USA. Phone: 617.632.5943; Email: cwu@partners.org.

MG's present address is: CeMM, Center for Molecular Medicine of the Austrian Academy of Sciences, Vienna, Austria.

L. Wang's present address is: Beckman Research Institute, City of Hope, Monrovia, California, USA.

1. Roberts AW, et al. Targeting BCL2 with venetoclax in relapsed chronic lymphocytic leukemia. *N Engl J Med*. 2016;374(4):311–322.
2. Pettijohn EM, Ma S. Targeted therapy in chronic lymphocytic leukemia (CLL). *Curr Hematol Malig Rep*. 2017;12(1):20–28.
3. Landau DA, et al. Mutations driving CLL and their evolution in progression and relapse. *Nature*. 2015;526(7574):525–530.
4. Puente XS, et al. Non-coding recurrent mutations in chronic lymphocytic leukaemia. *Nature*. 2015;526(7574):519–524.
5. Ferreira PG, et al. Transcriptome characterization by RNA sequencing identifies a major molecular and clinical subdivision in chronic lymphocytic leukemia. *Genome Res*. 2014;24(2):212–226.
6. Wang L, et al. SF3B1 and other novel cancer genes in chronic lymphocytic leukemia. *N Engl J Med*. 2011;365(26):2497–2506.
7. Darman RB, et al. Cancer-associated SF3B1 hotspot mutations induce cryptic 3' splice site selection through use of a different branch point. *Cell Rep*. 2015;13(5):1033–1045.
8. Alsafadi S, et al. Cancer-associated SF3B1 mutations affect alternative splicing by promoting alternative branchpoint usage. *Nat Commun*. 2016;7:10615.
9. DeBoever C, et al. Transcriptome sequencing reveals potential mechanism of cryptic 3' splice site selection in SF3B1-mutated cancers. *PLoS Comput Biol*. 2015;11(3):e1004105.
10. Wang L, et al. Transcriptomic characterization of SF3B1 mutation reveals its pleiotropic effects in chronic lymphocytic leukemia. *Cancer Cell*. 2016;30(5):750–763.
11. Alfarano A, et al. An alternatively spliced form of CD79b gene may account for altered B-cell receptor expression in B-chronic lymphocytic leukemia. *Blood*. 1999;93(7):2327–2335.
12. Ghassemifar R, et al. Differential expression of the Bcl-2 and Bax isoforms in CD19 positive B-lymphocytes isolated from patients diagnosed with chronic lymphocytic leukaemia. *Pathology*. 2012;44(7):632–637.
13. Morales AA, Olsson A, Celsing F, Osterborg A, Jondal M, Osorio LM. Expression and transcriptional regulation of functionally distinct Bmf isoforms in B-chronic lymphocytic leukemia cells. *Leukemia*. 2004;18(1):41–47.
14. Johnston HE, et al. Proteomics profiling of CLL versus healthy B-cells identifies putative therapeutic targets and a subtype-independent signature of spliceosome dysregulation. *Mol Cell Proteomics*. 2018;17(4):776–791.
15. Brooks AN, et al. Conservation of an RNA regulatory map between Drosophila and mammals. *Genome Res*. 2011;21(2):193–202.
16. Mi H, Muruganujan A, Thomas PD. PANTHER in 2013: modeling the evolution of gene function, and other gene attributes, in the context of phylogenetic trees. *Nucleic Acids Res*. 2013;41(Database issue):D377–D386.
17. Folco EG, Coil KE, Reed R. The anti-tumor drug E7107 reveals an essential role for SF3b in remodeling U2 snRNP to expose the branch point-binding region. *Genes Dev*. 2011;25(5):440–444.
18. Agrawal AA, et al. Novel SF3B1 in-frame deletions result in aberrant RNA splicing in CLL patients. *Blood Adv*. 2017;1(15):995–1000.
19. Akgul C, Moulding DA, Edwards SW. Alternative splicing of Bcl-2-related genes: functional consequences and potential therapeutic applications. *Cell Mol Life Sci*. 2004;61(17):2189–2199.
20. Kurtova AV, et al. Diverse marrow stromal cells protect CLL cells from spontaneous and drug-induced apoptosis: development of a reliable and reproducible system to assess stromal cell adhesion-mediated drug resistance. *Blood*. 2009;114(20):4441–4450.
21. Otake Y, et al. Overexpression of nucleolin in chronic lymphocytic leukemia cells induces stabilization of bcl2 mRNA. *Blood*. 2007;109(7):3069–3075.
22. Certo M, et al. Mitochondria primed by death signals determine cellular addiction to antiapoptotic BCL-2 family members. *Cancer Cell*. 2006;9(5):351–365.
23. Montero J, et al. Drug-induced death signaling strategy rapidly predicts cancer response to chemotherapy. *Cell*. 2015;160(5):977–989.
24. Larrayoz M, et al. The SF3B1 inhibitor spliceostatin A (SSA) elicits apoptosis in chronic lymphocytic leukaemia cells through downregulation of Mcl-1. *Leukemia*. 2016;30(2):351–360.
25. Deng J, Isik E, Fernandes SM, Brown JR, Letai A, Davids MS. Bruton's tyrosine kinase inhibition increases BCL-2 dependence and enhances sensitivity to venetoclax in chronic lymphocytic leukemia. *Leukemia*. 2017;31(10):2075–2084.
26. Bichi R, et al. Human chronic lymphocytic leukemia modeled in mouse by targeted TCL1 expression. *Proc Natl Acad Sci USA*. 2002;99(10):6955–6960.

27. Zanesi N, et al. Effect of rapamycin on mouse chronic lymphocytic leukemia and the development of nonhematopoietic malignancies in Emu-TCL1 transgenic mice. *Cancer Res*. 2006;66(2):915–920.
28. Johnson AJ, et al. Characterization of the TCL-1 transgenic mouse as a preclinical drug development tool for human chronic lymphocytic leukemia. *Blood*. 2006;108(4):1334–1338.
29. Yecies D, Carlson NE, Deng J, Letai A. Acquired resistance to ABT-737 in lymphoma cells that up-regulate MCL-1 and BFL-1. *Blood*. 2010;115(16):3304–3313.
30. Thijssen R, et al. Resistance to ABT-199 induced by microenvironmental signals in chronic lymphocytic leukemia can be counteracted by CD20 antibodies or kinase inhibitors. *Haematologica*. 2015;100(8):e302–e306.
31. Bojarczuk K, et al. BCR signaling inhibitors differ in their ability to overcome Mcl-1-mediated resistance of CLL B cells to ABT-199. *Blood*. 2016;127(25):3192–3201.
32. Khaw SL, et al. Both leukaemic and normal peripheral B lymphoid cells are highly sensitive to the selective pharmacological inhibition of prosurvival Bcl-2 with ABT-199. *Leukemia*. 2014;28(6):1207–1215.
33. ten Hacken E, et al. Targeting the LYN/HS1 signaling axis in chronic lymphocytic leukemia. *Blood*. 2013;121(12):2264–2273.
34. Kotschy A, et al. The MCL1 inhibitor S63845 is tolerable and effective in diverse cancer models. *Nature*. 2016;538(7626):477–482.
35. Souers AJ, et al. ABT-199, a potent and selective BCL-2 inhibitor, achieves antitumor activity while sparing platelets. *Nat Med*. 2013;19(2):202–208.
36. Sveen A, Kilpinen S, Ruusulehto A, Lothe RA, Skotheim RI. Aberrant RNA splicing in cancer; expression changes and driver mutations of splicing factor genes. *Oncogene*. 2016;35(19):2413–2427.
37. Agrawal AA, Yu L, Smith PG, Buonamici S. Targeting splicing abnormalities in cancer. *Curr Opin Genet Dev*. 2018;48:67–74.
38. Lee SC, Abdel-Wahab O. Therapeutic targeting of splicing in cancer. *Nat Med*. 2016;22(9):976–986.
39. Salton M, Misteli T. Small molecule modulators of pre-mRNA splicing in cancer therapy. *Trends Mol Med*. 2016;22(1):28–37.
40. Liu Y, et al. Impact of alternative splicing on the human proteome. *Cell Rep*. 2017;20(5):1229–1241.
41. Lee SC, et al. Modulation of splicing catalysis for therapeutic targeting of leukemia with mutations in genes encoding spliceosomal proteins. *Nat Med*. 2016;22(6):672–678.
42. Obeng EA, et al. Physiologic expression of Sf3b1(K700E) causes impaired erythropoiesis, aberrant splicing, and sensitivity to therapeutic spliceosome modulation. *Cancer Cell*. 2016;30(3):404–417.
43. Xargay-Torrent S, et al. The splicing modulator sudemycin induces a specific antitumor response and cooperates with ibrutinib in chronic lymphocytic leukemia. *Oncotarget*. 2015;6(26):22734–22749.
44. Kumar D, et al. Selectivity in small molecule splicing modulation. *ACS Chem Biol*. 2016;11(10):2716–2723.
45. Kashyap MK, et al. Targeting the spliceosome in chronic lymphocytic leukemia with the macrolides FD-895 and pladienolide-B. *Haematologica*. 2015;100(7):945–954.
46. Dvinge H, Bradley RK. Widespread intron retention diversifies most cancer transcriptomes. *Genome Med*. 2015;7(1):45.
47. Patel VK, et al. Pharmacodynamics and proteomic analysis of acalabrutinib therapy: similarity of on-target effects to ibrutinib and rationale for combination therapy. *Leukemia*. 2018;32(4):920–930.
48. Del Gaizo Moore V, Brown JR, Certo M, Love TM, Novina CD, Letai A. Chronic lymphocytic leukemia requires BCL2 to sequester prodeath BIM, explaining sensitivity to BCL2 antagonist ABT-737. *J Clin Invest*. 2007;117(1):112–121.
49. Davids MS, et al. Decreased mitochondrial apoptotic priming underlies stroma-mediated treatment resistance in chronic lymphocytic leukemia. *Blood*. 2012;120(17):3501–3509.
50. Hong DS, et al. A phase I, open-label, single-arm, dose-escalation study of E7107, a precursor messenger ribonucleic acid (pre-mRNA) splicesome inhibitor administered intravenously on days 1 and 8 every 21 days to patients with solid tumors. *Invest New Drugs*. 2014;32(3):436–444.
51. Ten Hacken E, et al. Functional differences between IgM and IgD signaling in chronic lymphocytic leukemia. *J Immunol*. 2016;197(6):2522–2531.
52. Foight GW, Ryan JA, Gullá SV, Letai A, Keating AE. Designed BH3 peptides with high affinity and specificity for targeting Mcl-1 in cells. *ACS Chem Biol*. 2014;9(9):1962–1968.
53. Dutta S, Ryan J, Chen TS, Kougentakis C, Letai A, Keating AE. Potent and specific peptide inhibitors of human pro-survival protein Bcl-xL. *J Mol Biol*. 2015;427(6 Pt B):1241–1253.
54. Jenson JM, Ryan JA, Grant RA, Letai A, Keating AE. Epistatic mutations in PUMA BH3 drive an alternate binding mode to potently and selectively inhibit anti-apoptotic Bfl-1. *Elife*. 2017;6.
55. Morciano G, et al. Mcl-1 involvement in mitochondrial dynamics is associated with apoptotic cell death. *Mol Biol Cell*. 2016;27(1):20–34.
56. Zhao JJ, et al. Targeting the miR-221-222/PUMA/BAK/BAX pathway abrogates dexamethasone resistance in multiple myeloma. *Cancer Res*. 2015;75(20):4384–4397.
57. Sewastianik T, et al. Constitutive Ras signaling and Ink4a/Arf inactivation cooperate during the development of B-ALL in mice. *Blood Adv*. 2017;1(25):2361–2374.